Temporally Compound Heatwave and Its Interaction With Urban Heat Island Over Mainland China

Zhang, Liwei; Liao, Weilin; Chen, Xuan; Cheng, Shanjun; Yang, Jiachuan

DOI
10.1029/2025EF006490

Publication date
2025

Document Version
Final published version

Published in
Earth's Future

Citation (APA)
Zhang, L., Liao, W., Chen, X., Cheng, S., & Yang, J. (2025). Temporally Compound Heatwave and Its Interaction With Urban Heat Island Over Mainland China. *Earth's Future*, *13*(8), Article e2025EF006490. https://doi.org/10.1029/2025EF006490

Earth's Future

RESEARCH ARTICLE
10.1029/2025EF006490

Temporally Compound Heatwave and Its Interaction With Urban Heat Island Over Mainland China

Liwei Zhang[1], **Weilin Liao**[2], **Xuan Chen**[3], **Shanjun Cheng**[4], **and Jiachuan Yang**[1]

[1]Department of Civil and Environmental Engineering, The Hong Kong University of Science and Technology, Hong Kong, China, [2]Guangdong Key Laboratory for Urbanization and Geo-simulation, School of Geography and Planning, Sun Yat-sen University, Guangzhou, China, [3]Department of Water Management, Delft University of Technology, Delft, the Netherlands, [4]Tianjin Climate Center, Tianjin, China

Abstract Temporally compound heatwaves (CHWs), two consecutive heatwaves (HWs) with an intermittent cool break between them, are projected to occur more frequently under a warming globe. However, their spatiotemporal characteristics and interaction with urban heat island (UHI) are unexplored at the continental scale. Using observational data from over 2000 ground-based stations over China, we find that CHWs constitute an increasing portion of HW hazard from 1961 to 2021. The increasing trend is especially evident when using the daily minimum temperature to define hot days, suggesting an aggravated thermal environment at night. Urban-rural contrast of CHW trends illustrates that urbanization contributes substantially to the increased frequency of CHWs in cities, especially in southern China. Results show that mean UHI intensity (UHII) tends to weaken under HW and CHW conditions, which correlates with increased pressure and reduced precipitation. During CHW events, UHII reduces during cool break due to enhanced evaporative cooling in urban areas under precipitation. The interaction between UHI and HW is subject to change with background climate, which is positive for dry regions and negative for wet regions. This study provides insights into CHW evolution over mainland China and demonstrates the need for heat mitigation strategies under climate change.

Plain Language Summary Temporally compound heatwaves (CHWs) are defined as two consecutive heatwaves (HWs) separated by a cool break. However, their characteristics and interaction with urban heat island (UHI) have not been explored before. In this study, we analyze the temperature data from over 2000 weather stations in mainland China. We find that CHWs are becoming a growing threat from 1961 to 2021, particularly at night. Due to the contributions of urbanization, the urban areas experience CHWs more frequently than rural areas, especially in southern China. The UHI intensity (UHII) reduces during CHWs over mainland China, which is likely due to the increased pressure and reduced precipitation. During CHWs, the lowest UHIIs occur at cool break and are attributed to the high frequency of precipitation. Policy makers could refer to these findings and take desirable mitigation measures to cope with prolonged heat stress in the future.

Key Points:

- Frequency and duration of compound heatwaves (CHWs) exhibit significant increasing trends over China during 1961–2021
- Urbanization contributes to the increased frequency of CHWs, especially in southern China
- UHII tends to reduce and have a larger variability under CHWs

Supporting Information:

Supporting Information may be found in the online version of this article.

Correspondence to:

J. Yang,
cejcyang@ust.hk

Citation:

Zhang, L., Liao, W., Chen, X., Cheng, S., & Yang, J. (2025). Temporally compound heatwave and its interaction with urban heat island over mainland China. *Earth's Future*, *13*, e2025EF006490. https://doi.org/10.1029/2025EF006490

Received 23 APR 2025
Accepted 14 JUL 2025

Author Contributions:

Conceptualization: Liwei Zhang, Jiachuan Yang
Data curation: Weilin Liao, Shanjun Cheng
Formal analysis: Weilin Liao
Funding acquisition: Jiachuan Yang
Methodology: Liwei Zhang, Weilin Liao, Xuan Chen, Jiachuan Yang
Supervision: Jiachuan Yang
Writing – original draft: Liwei Zhang, Jiachuan Yang
Writing – review & editing: Xuan Chen, Shanjun Cheng, Jiachuan Yang

1. Introduction

Global warming has led to a rapid increase in the magnitude and frequency of heatwave (HW), which is characterized by high atmospheric pressure and elevated temperature across a large region, posing severe threats to human health and natural systems (Perkins-Kirkpatrick & Lewis, 2020; P. Wang et al., 2017; S. Wu et al., 2023). For instance, the European continent suffered over 70,000 deaths from a devastating HW during the summer of 2023 (Robine et al., 2008). France suffered a HW with a highest temperature of 45.9°C in 2019, exceeding the country's highest temperature record (Mitchell et al., 2019). Since the mid-20th century, HWs have generally increased and intensified over China. A total of 16,299 deaths and an overall economic loss of 61,304 million RMB were attributed to HWs in 2017 (Yan et al., 2022). In late June 2021, an unprecedented HW struck British Columbia, Canada, resulting in a 31% reduction in spring wheat production, a 30% decrease in barley, and a 21% decline in canola yields (White et al., 2023). It is therefore imperative to investigate the spatiotemporal characteristics of HWs.

Previous studies have investigated the spatiotemporal characteristics of HWs around the globe, such as Africa (Ceccherini et al., 2017; Meque et al., 2022), Aisa (Y. Chen & Zhai, 2017; Chew et al., 2021), Oceania (Jyoteeshkumar Reddy et al., 2021; Perkins-Kirkpatrick et al., 2016), and America (Peterson et al., 2013; Thompson et al., 2022). As one of the most densely populated countries in the world, China has been hit by severe and

frequent HW events in recent decades (Ding & Chen, 2024; Kong et al., 2020; W. Wang et al., 2013). You et al. (2017) found that southern China has the highest number of HW days due to rapid urbanization since 1990. Liao et al. (2018) found the increasing trend of HWs in urban areas are more prominent than in rural areas of the Pearl River Delta. Ye et al. (2018) reported that urbanization contributes to 0.44 events decade^{-1} and 3.96 days decade^{-1} in southern China.

Despite the large number of studies in the literature, existing studies focused on isolated HW events defined by a threshold temperature and duration. Anderson and Bell (2011) defined HW as a period of two or more consecutive days with a daily minimum temperature greater than the 95th percentile temperature threshold. J. Wang et al. (2020) defined HW as a period of at least three consecutive hot days with a daily maximum temperature greater than the 90th percentile temperature threshold. Recently, Baldwin et al. (2019) found that temporally compound heatwave, two consecutive HWs separated by a cool break, will constitute a significant proportion of future HW hazards. As an extended long period of hazards, CHWs (temporally compound heatwaves) may cause a high mortality rate due to subsequent temperature extremes following an initial HW. However, the spatiotemporal characteristics of CHW and their patterns in urban and rural areas remain largely unclear at continental scales.

Due to rapid urbanization in the past decades, global cities have witnessed higher temperatures than their surrounding rural areas, a phenomenon widely known as the urban heat island (UHI) effect (Stewart, 2011). UHIs can interact with HW and result in magnified heat hazards within cities. Such interactions between HW and UHI can vary substantially from city to city, and change across the diurnal cycle. Jiang et al. (2019) reported that daytime UHII in Beijing and Shanghai increased by 0.2 and 0.9°C, respectively, during HWs, but the daytime UHII in Guangzhou reduced by 0.2°C. Meanwhile, nocturnal UHIIs consistently intensify during HWs across different climate regions (Jiang et al., 2019; Zhao et al., 2018). Physical processes and driving factors responsible for the changes of UHIIs under HWs also differ from city to city. Li and Bou-Zeid (2013) suggested that the intensification of UHII during HWs in Washington, USA, can be attributed to the low wind speed during HWs and the lack of surface moisture in urban areas. Ao et al. (2019) found that amplified energy storage in built surfaces with anthropogenic heat emissions are the major driver for the synergistic interaction between UHI and HWs in Beijing, China. Thermal memory can likely maintain a warm urban environment during the short cool breaks of CHWs and change urban-rural temperature difference after the breaks. Nevertheless, the interaction between CHW and UHI has not yet been investigated.

In this study, we aim to quantify the spatiotemporal characteristics of CHW in mainland China using observational surface air temperature data set. Are there any interactions between UHI and CHWs? What are the physical mechanisms that govern the interaction? We will use different temperatures to address these questions. Results are expected to have important implications for resilient urban thermal environment under the challenges of climate change.

2. Methods

2.1. Data

Daily maximum, mean and minimum temperatures, precipitation (PRE), wind speed (WIN), sea level pressure (PRS), and relative humidity (RHU) were collected from 2,419 national standard meteorological stations in mainland China from 1961 to 2021 in this study. With a focus on HW, we analyzed the data in warm months (May to September). The raw temperature records have been homogenized using the method described by Xu et al. (2013). Stations will be discarded with 5% or more missing data in any year during the study period.

To explore the effects of urbanization on CHW events, land use data was used to classify urban and rural stations. Following the previous studies (Liao et al., 2018; Ren & Zhou, 2014), we adopted a dynamic classification method based on the land use maps in different subperiods. Time-varying land use maps of China generated using Landsat TM/ETM + images with a spatial resolution of 30 m were used in this study (J. Liu et al., 2014). These maps are provided by the Data Center for Resources and Environmental Sciences, Chinese Academy of Sciences (RESDC, 2024) and are available for seven episodes (1980, 1990, 1995, 2000, 2005, 2010, and 2015). According to these maps, the study period 1961–2021 was divided into seven subperiods, 1961–1980, 1981–1990, 1991–1995, 1996–2000, 2001–2005, 2006–2010, and 2011–2021. The division of subperiods is based on China's urban expansion trends. According to F. Liu et al. (2021), before 1980, China's urban expansion was very slow. From 1980 to 1990, the urban expansion was slow but stable. After 1990, the urbanization pace increased,

continuing at a high speed until 2000s. Then the speed of urban expansion slowed down after 2015. The fraction of built-up area for each subperiod was calculated using the map at the end of the period, except for the last subperiod when the built-up area was determined using the 2015 map.

The fraction of built-up area in a circular buffer centered at individual stations with a radius of 2 km was calculated (Ren & Zhou, 2014). If the fraction is greater than or equal to 33%, the station is classified as an urban station, otherwise, it is treated as a rural station. Figure S1 in Supporting Information S1 shows the spatial distribution of urban and rural stations in different periods. In the period from 1980 to 2015, 901 rural stations were converted to urban stations, and the ratio of urban stations reached 46.3% in 2015.

2.2. Definition of CHW

HW is typically defined as a period of at least three consecutive hot days with temperatures above a threshold value. Following previous studies, here we adopted three definitions to estimate the temperature threshold values for defining a hot day (Anderson & Bell, 2011; Y. Chen & Zhai, 2017; Ren & Zhou, 2014):

1. 90th percentile of all daily temperatures during warm months from 1961 to 1990. The threshold value will not change with time for individual grid.
2. 90th percentile of the daily temperatures within 15-day moving window during warm months from 1961 to 1990. The threshold value will change from day-to-day and is computed using a total sample of 450 days for each calendar day (15-day window per year times 30 years). Compared to definition (1), this definition accounts for climate dynamics through incorporating monthly and daily temperature variations into estimating the threshold.
3. 90th percentile of the daily temperatures within 15-day moving window during warm months from 1961 to 2021. This definition is similar to definition (2), but with a period of 1961–2021 to account for the global warming trend.

After determining the hot days, the next step is to find the CHW events. Following the definitions by Baldwin et al. (2019), a CHW is defined as two consecutive HWs with a cool break. It usually constitutes the following periods: (a) a minimum number of consecutive hot days, (b) a maximum number of cool days, and (c) a minimum number of hot days after the cool break. To obtain a large sample size of CHWs, we define a CHW event with a minimum length of three hot days, a maximum length of three cool days as the break, and a minimum of length of three consecutive days after the cool break. Note that 90th percentile temperature is adopted to include a large sample size of CHWs in our analyses, additional sensitivity tests show that the trend of CHW characteristics are qualitatively similar when using 95th percentile as the threshold values (Figures S8–S10 in Supporting Information S1). In addition, maximum, mean and minimum temperatures are used to explore whether the results depend on the type of temperatures. As a result, we have a total of nine definitions for a CHW event, as shown in Table S1 in Supporting Information S2. In this study, three indicators are used to investigate the CHW characteristics: the number of CHW events (CHWN), the duration of CHW (CHWD), and the highest temperature during CHW (CHWT). It is noteworthy that if three heatwaves are connected by two cool breaks, they will be counted as two distinct CHW events, and so forth. When calculating the total duration of CHW, however, each hot day will only be counted once.

2.3. Urban-Rural Contrast of CHW

Note that HWs are large-scale weather events that shall be identified from synoptic background conditions rather than at individual stations. Because urban stations are under the influence of anthropogenic activities, here we adopted the rural stations to estimate the temperature threshold value for determining HW. According to the site selection criteria by China Meteorological Administration (https://www.cma.gov.cn), rural weather stations are situated in natural open areas with a radius of 20 km. This suggests that the rural stations are not influenced by anthropogenic activities and their recorded data can be used to determine the threshold values. The threshold value is computed as the mean rural temperature over 5° × 5° grids across mainland China (Figure S1 in Supporting Information S1). To eliminate the effects of elevation, stations will be discarded if their elevations are more than 250 m away from the grid mean, which leaves a total of 1,741 stations (urban and rural) for this study. There are 32 grids with at least one urban and one rural station over the study area during all subperiods. As the temperature threshold values are grid-based, we tested different grid divisions to ensure the robustness of our results (4° × 4° longitude and latitude grid in Figure S2 in Supporting Information S1).

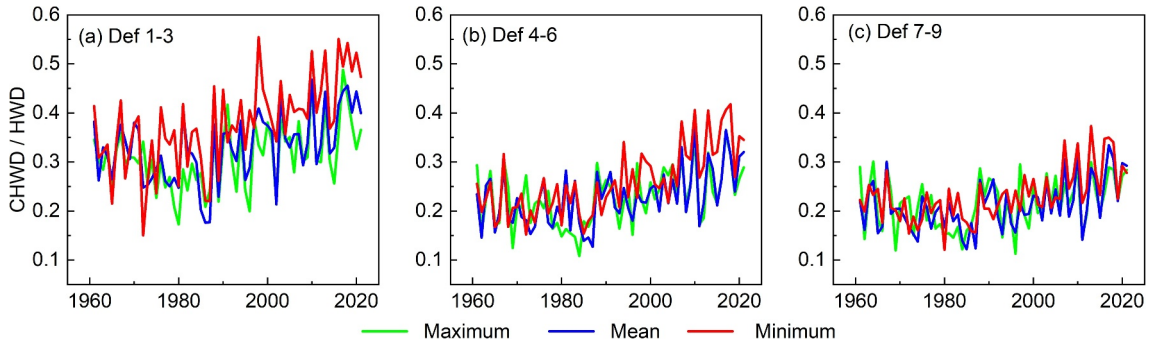

Figure 1. Trends of CHWD/HWD during 1961–2021 under nine definitions, (a) Def 1–3, (b) Def 4–6, and (c) Def 7–9.

To investigate the differences of CHW characteristics between urban and rural areas: First, the time series of mean urban and mean rural temperatures at individual grids were constructed by averaging data from all urban and rural stations in one grid. Second, based on the time series of mean rural temperature, the temperature threshold values were determined by the proposed definition (1)–(3) in Section 2.2. Finally, HW and CHW events were identified for all stations in each year. The characteristics of CHW (i.e., CHWN, CHWD and CHWT) were averaged at the grid level to investigate the urban and rural trends. In this study, UHII is defined as the daily air temperature difference between urban and rural areas, which is computed using the time series of mean urban temperatures and mean rural temperatures at the grid level. When HW (non-HW) periods are different in urban and rural time series, estimated UHIIs are discarded.

3. Results and Discussion

3.1. Long-Term Trend of CHWs

To investigate the long-term trend of CHWs, we first look into the ratios between CHW days and HW days (CHWD/HWD) with different definitions. Note that CHWD equals to the sum of hot days in two HWs during a CHW event. As shown in Figure 1, the CHWD/HWD ratios show an increasing trend from 1961 to 2021, suggesting that a larger portion of HWs becomes temporally compound in the past few decades. One plausible explanation is that as temperature rises, the water-hold capacity of air increases and HW may dry out the land surface more substantially (Baldwin et al., 2019). Reduced soil moisture on land will facilitate the formation of subsequent heat events as evaporation cooling mechanism diminishes. As a result, HWs may become more likely to cluster and compound. When using the same temperature type to define HWs, the increasing trend is consistent across different threshold values. For example, when using the mean temperatures, the increasing rate is 0.017, 0.016 and 0.012 decade^{-1} under different threshold values. Average CHWD/HWD values are 0.34, 0.24 and 0.22 under threshold definitions (1), (2), and (3), respectively. The larger CHWD/HWD value under definitions (2) than under definition (3) indicates that ignoring global warming trend can lead to a slight overestimation of CHWs. And the large difference in CHWD/HWD value between definition (1) and definition (2) suggests that CHWs will be substantially overestimated if climate dynamics are ignored when identifying HWs. This analysis highlights the importance of accounting for both intra-seasonal variability and global warming when assessing CHW trends.

When using the maximum, mean and minimum temperatures to define CHWs, the average increases of CHWD/HWD from 1961 to 2021 are 15.2%, 20.9%, and 31.4%, respectively. Regardless of the threshold values, it can be observed that CHWD/HWD is the largest when HW is defined using daily minimum temperature. This is due to a more rapid increase of the daily minimum temperature than the daily mean and maximum values, which has been reported from Liao et al. (2018). We therefore adopt the minimum temperatures to analyze the spatial distribution of CHW characteristics in subsequent analysis. Using the Def 9 of CHW (Table S1 in Supporting Information S2), the spatial distribution of the characteristics of CHW over mainland China is shown in Figure S3 in Supporting Information S1, including the growth rate of CHWN (Figure S3a in Supporting Information S1), CHWD (Figure S3b in Supporting Information S1) and CHWT (Figure S3c in Supporting Information S1). It is evident that CHW events have become more frequent in most regions of mainland China, and the trend is consistent when using different grid divisions (Figures S3d–S3f in Supporting Information S1).

10.1029/2025EF006490

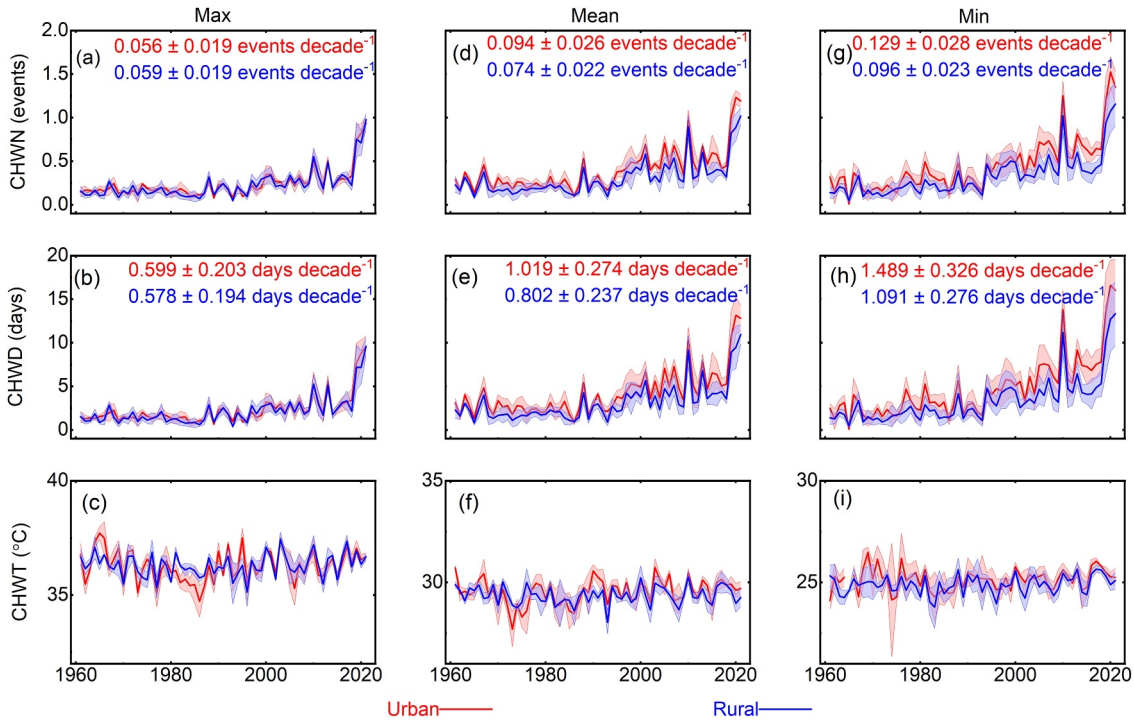

Figure 2. Temporal trend of CHW characteristics in urban and rural areas during 1961–2021. Results based on (a)–(c) daily maximum temperature, Def 1, Def 4, and Def 7; (d)–(f) daily mean temperatures, Def 2, Def 5, and Def 8; (g)–(i) daily minimum temperatures, Def 3, Def 6, and Def 9. The shading part represents the mean ± standard deviation among the definitions with three different temperature threshold values.

3.2. Urban-Rural Contrast of CHW Trend

After investigating the spatiotemporal distribution of CHW characteristics, we compared their evolution in urban and rural areas in this section. Figure 2 presents the trends of CHWN, CHWD and CHWT. It can be found that CHWN and CHWD show an increasing trend in both urban and rural areas during 1961–2021, regardless of the definitions. When using mean and minimum temperature definitions, CHWN and CHWD in urban areas are higher than those in rural areas (Figures 2d, 2e, 2g, and 2h), while results based on maximum temperature show negligible differences. The negligible urban-rural difference based on daily maximum temperature is caused by small UHII during daytime. Daily maximum temperature typically occurs in early afternoon when strong solar radiation creates urban-rural circulation. The mixing process by circulation leads to small air temperature differences between urban and rural areas. As a result, air temperature based UHI is much smaller during daytime than at night. For example, Sarangi et al. (2021) reported that night-time UHI varied from 1.6 to 4.8°C and daytime UHI varied from −0.7 to 1.4°C in Eastern US cities.

The urban-rural difference of CHWN and CHWD trend reaches the maximum of 0.033 events decade^{-1} and 0.399 days decade^{-1} under the minimum temperature definition. A large urban-rural difference of CHW events demonstrates a significant contribution of the urbanization to the CHW event frequency. It is noteworthy that urban-rural difference becomes evident after 1990, which coincides with the period of rapid urbanization in China (M. Chen et al., 2013; Yao et al., 2022). For example, the urban-rural difference of CHWN is 0.007 events decade^{-1} during 1961–1990, and increases to 0.081 events decade^{-1} during 1991–2021 (Figure 2g). Similarly, the urban-rural difference of CHWD is 0.174 days decade^{-1} before 1990 and is 0.932 days decade^{-1} after 1990 (Figure 2h).

Figure S3c in Supporting Information S1 shows an increasing trend of CHWT in most stations, while the increasing trends of CHWT in urban and rural areas are not so clear (Figures 2c, 2f, and 2i). The reason is that rural stations are reclassified as urban stations as time goes during the study period. Because urban CHWTs are typically higher than rural CHWTs (see Figure 2i during 1961–1980), this can diminish the increasing trend of grid-based CHWTs in urban areas. The reduction in the number of rural stations also contributes to this diminishing trend. Consequently, the overall trend in CHWT does not indicate a significant increase over the study period.

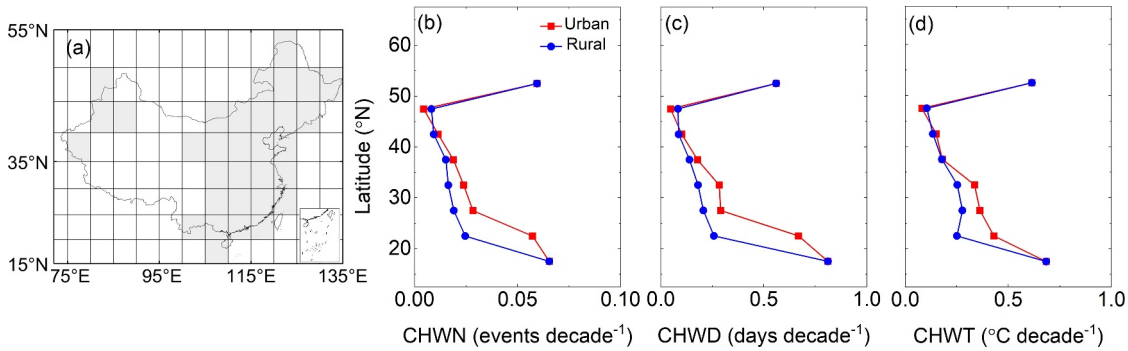

Figure 3. (a) Divided grids of 5° × 5° latitude-longitude, and gray grids represent these grids with at least one urban and rural station. The urban-rural contrasts of average increasing rates in (b) CHWN, (c) CHWD, and (d) CHWT are the results calculated from the increasing rates of these grids within the same latitudes.

As CHW events have a cool break between two HWs, we examined whether the length of cool break will affect the urban-rural difference. Across all lengths of cool break, urban areas consistently show a larger increasing trend of CHWN and CHWD than rural regions based on definitions with daily mean and daily minimum temperatures (Figures S4 and S5 in Supporting Information S1). Interesting, the urban-rural difference becomes smaller with a shorter cool break. The urban-rural difference of CHWN and CHWD is 0.024 events decade^{-1} (Figure S4g in Supporting Information S1) and 0.322 days decade^{-1} (Figure S4h in Supporting Information S1) for a cool break ≤2 days, while it is 0.012 events decade^{-1} (Figure S5g in Supporting Information S1) and 0.196 days decade^{-1} (Figure S5h in Supporting Information S1) for a cool break of 1 day. One plausible explanation for this phenomenon is that urban areas have higher thermal inertia than rural areas and thus can retain heat for a longer time. As the cool break extends from 1 day to 3 days, the CHW events increase more in urban areas than in rural areas, leading to a larger urban-rural difference.

We further investigated the spatial distribution of urban-rural contrast across mainland China in Figure 3. Under def 9, Figures 3b–3d show that urban-rural difference of CHWN, CHWD and CHWT is more evident in southern China. And small differences are found in areas with a latitude smaller than 20° due to few stations in that grid. The large urban-rural difference in Southern China is caused by higher urbanization rate in this region, especially in the Pearl River Delta and the Yangtze River Delta (X. Wu et al., 2020; Ye et al., 2018). It is worth pointing out that the frequency and duration of CHW increase slightly faster in rural areas than in urban areas at latitudes 45°–50°. This region includes parts of Northeast and Northwest China where urban expansion is lower than the national average (F. Liu et al., 2021), leading to smaller urban-rural difference in CHW characteristics. The same analysis is repeated for 4° × 4° grids, and the urban-rural contrast remains largely consistent (see Figure S6 in Supporting Information S1).

Additionally, to better understand the temporal evolution of urban-rural contrast of CHW characteristics, we analyzed the correlation between the urbanization rate and urban-rural differences of CHWN and CHWD during seven subperiods. Because the differences in CHWs when defined by the maximum temperature are trivial, we computed the average urban-rural differences using mean and minimum temperature definitions. The ratio of urban stations among all stations was used to reflect the urbanization rate at different subperiods. The urban-rural contrast in CHWD and CHWN shows a strong correlation ($r > 0.8$, $p < 0.05$) with the urbanization rate (see Figure S7 in Supporting Information S1). Notably, in the last three subperiods (2001–2021), the urban-rural contrast evidently intensifies compared to the periods before the 2000s. Urbanization leads to an increase in impervious surfaces and a decrease in green spaces, resulting in rising urban temperatures due to reduced evaporative cooling (Deng et al., 2009; Zhou et al., 2025).

3.3. Interaction Between CHW and UHI

Until now, our analyses have demonstrated the urban-rural difference of CHW characteristics, yet it remains unclear how such difference will modify the UHII. Considering the CHW events are far fewer during 1961–1990 than in 1991–2021 (as depicted in Figure 2), our analyses of UHI in this section will focus on 1991–2021.

Figure 4a shows that UHIIs are much larger on non-HW days than on HW and CHW days at the continental scale, and the trend is consistent among three temperature types. Note that this finding is not in contradiction with

10.1029/2025EF006490

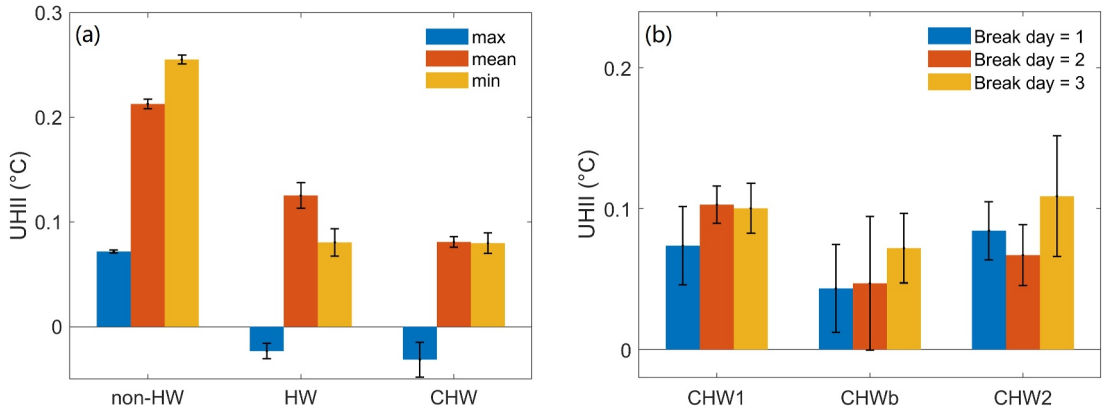

Figure 4. (a) Average UHII on non-HW, HW and CHW days during 1991–2021. (b) Average UHII based on mean temperature definitions under different length of cool break during 1991–2021.

previous studies reporting synergistic interactions between UHI and HW during a single event or at individual cities. Various studies in literature have reported different interactions between UHI and HW at different cities and at different times of the day. For example, UHII was slightly reduced during the daytime under HW compared to non-HW conditions in Guangzhou (G. Chen et al., 2023; Jiang et al., 2019). However, a synergistic interaction between UHI and HW is verified in summer in Shanghai, which is strong at the coastal site but remains strong during daytime under sunny days at the inland site (Ao et al., 2019). Tian et al. (2021) found the UHII to be 0.5°C higher during HW periods than under normal conditions in Chongqing during 1979–2018. Our subsequent analyses in wet and dry regions also demonstrate that the interaction between UHI and CHW depends on the background weather.

Another interesting question is how UHI temporally evolve during the CHW events with different lengths of cool break. Figure 4b shows that UHII is smaller during the cool break than under hot days in CHWs. It can be found the average precipitation and RHU are higher during cool break (70.0%, 6.5 mm) than under the first HW (CHW1: 61.1%, 1.1 mm) and the second HW (CHW2: 61.7%, 1.3 mm), while the difference of pressure at sea level and wind speed is small (Figure S11 in Supporting Information S1). Previous studies observed a large probability of extreme precipitation after a HW event, especially in the mid-latitude regions (Sauter et al., 2023; S. Wu et al., 2021). In our study, we also found that about 45% of cool break periods during CHWs have experienced rainfall. During the short cool break with rainfall, urban areas with large impervious surfaces can have comparable evaporation with rural areas, which leads to smaller urban-rural temperature difference (P. Yang et al., 2019). The reduced UHII during cool break is consistently found with different lengths of cool break. And UHII remains largely unchanged with different lengths of cool break.

Note that daily maximum and minimum temperatures only reflect the thermal conditions at a short period of the day, while mean temperature can represent the overall conditions over the diurnal cycle. As shown in Figure 2, urban and rural regions show negligible differences in CHW characteristics when using daily maximum temperature definitions. To better understand the effects of synoptic background conditions on the UHII variations, we examined the relationship between UHII based on daily mean temperatures and different meteorological parameters. Figure 5 shows the correlation between mean UHII and mean RHU, PRS, PRE, and WIN during the warm months (May–September) at each year over the entire China. Note that the mean RHU, PRS, PRE and WIN are averaged over all stations (including both urban and rural ones) to represent the background climate. It is found that UHI is positively correlated with RHU ($r = 0.32$, $p < 0.01$) and PRE ($r = 0.45$, $p < 0.01$), and negatively correlated with PRS ($r = -0.42$, $p < 0.01$) and WIN ($r = -0.33$, $p < 0.01$). Figure 5 shows that UHII has a negative relationship with PRS, as HW generally comes with a high-pressure system (Ramamurthy & Bou-Zeid, 2017). The high-pressure system tends to result in divergent flows and clear days with no precipitation, and as a result, UHII has a positive correlation with daily mean PRE. The positive relationship is consistent with the trend found over US cities by Zhao et al. (2014). During the warm months, large precipitation increases soil moisture in rural areas under non-HW days. This allows more radiation partition into latent heat in rural areas, creating a strong urban-rural difference in evaporation and consequently a higher UHI on non-HW days. The relationship between UHII and PRS/PRE remain quantitively the same when using different definitions (Table S2

10.1029/2025EF006490

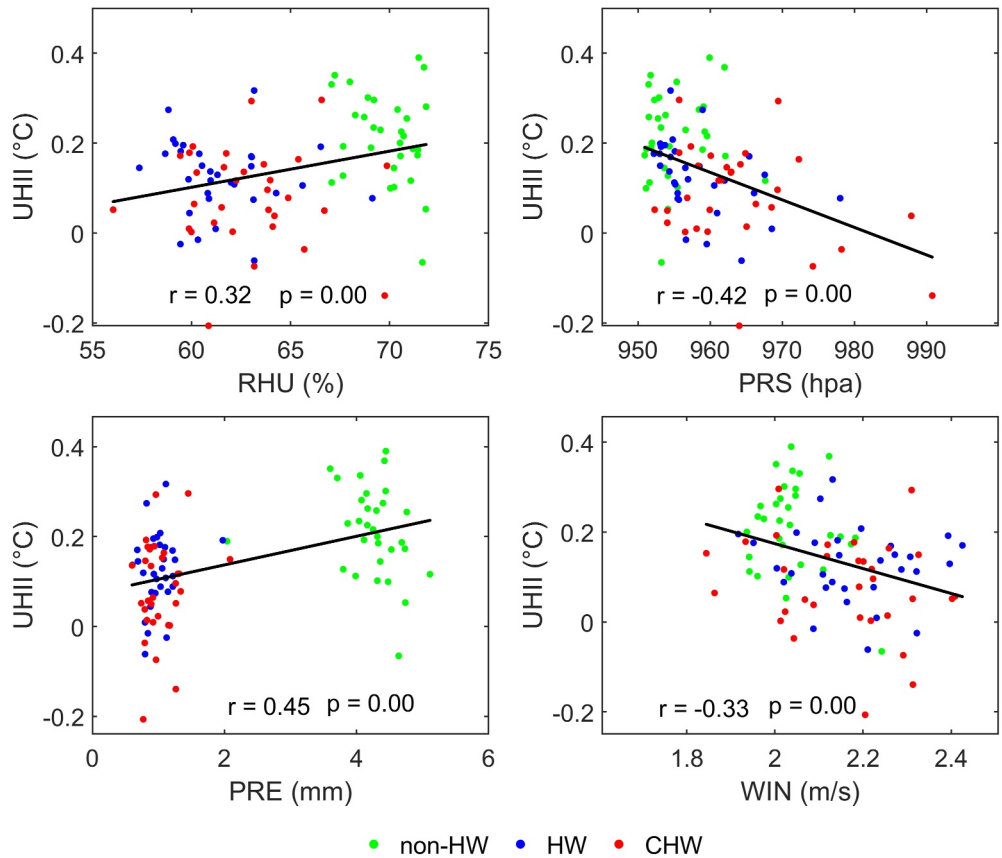

Figure 5. Relationship between mean UHIIs (based on three different threshold definitions under mean temperatures) of warm months and the corresponding RHU, PRS, PRE, and WIN on non-HW, HW and CHW conditions during 1991–2021. The red, blue and green dots represent CHW, HW and non-HW conditions, respectively.

in Supporting Information S2). Wind speed is higher under HW and CHW conditions than under non-HW conditions, which enhances urban-rural mixing and reduces the temperature gradient, thus alleviating the UHI (Li et al., 2016).

To examine whether the interaction between UHI and CHW changes with background climate, a wet grid (110°–115°E, 20°–25°N) and a dry grid (110°–115°E, 35°–40°N) are selected. The classification of dry and wet regions depends on mean daily PRE over all stations within each grid during warm months, with dry areas having a mean daily PRE <3 mm and wet areas ≥3 mm. This classification allows us to capture the general characteristics of wet and dry regions. The PRE and RHU of the wet grid (7.83 mm, 80.5%) is much larger than the dry grid (2.47 mm, 63.3%). Figure 6a shows that distribution of UHII on non-HW days has a larger mean value than that on HW days in wet areas. However, in dry areas, Figure 6b illustrates that UHII is slightly intensified on HW days compared to non-HW days. The UHI is caused by urban-rural difference in evapotranspiration, which is supported by abundant moisture under non-HW days in wet regions. Under HW conditions, synoptic forcing results in temporally dry conditions that reduces the urban-rural difference in evapotranspiration. As a result, UHII reduces under HW conditions in wet regions. On the contrary, dry regions feature low moisture availability and UHI is mainly caused by urban-rural difference in thermal inertia. Under hot conditions caused by HWs, the urban-rural temperature difference (i.e., UHI) will be further increased. It is worth mentioning that the distribution of UHII is wider with a lower peak under CHW than on HW, for both wet and dry regions. This is because cool breaks during CHWs have distinct meteorological conditions from hot days, which complicates the dynamics of urban air temperature and yields a larger span of UHII.

To assess the robustness of our results, we examined the interactions between UHI and HW/CHW across all grids. Figures 6c and 6d show that ΔUHII (mean UHII during HW/CHW minus that under non-HW days) exhibits a decreasing trend with mean PRE during warm months, although this trend is not statistically significant. When

10.1029/2025EF006490

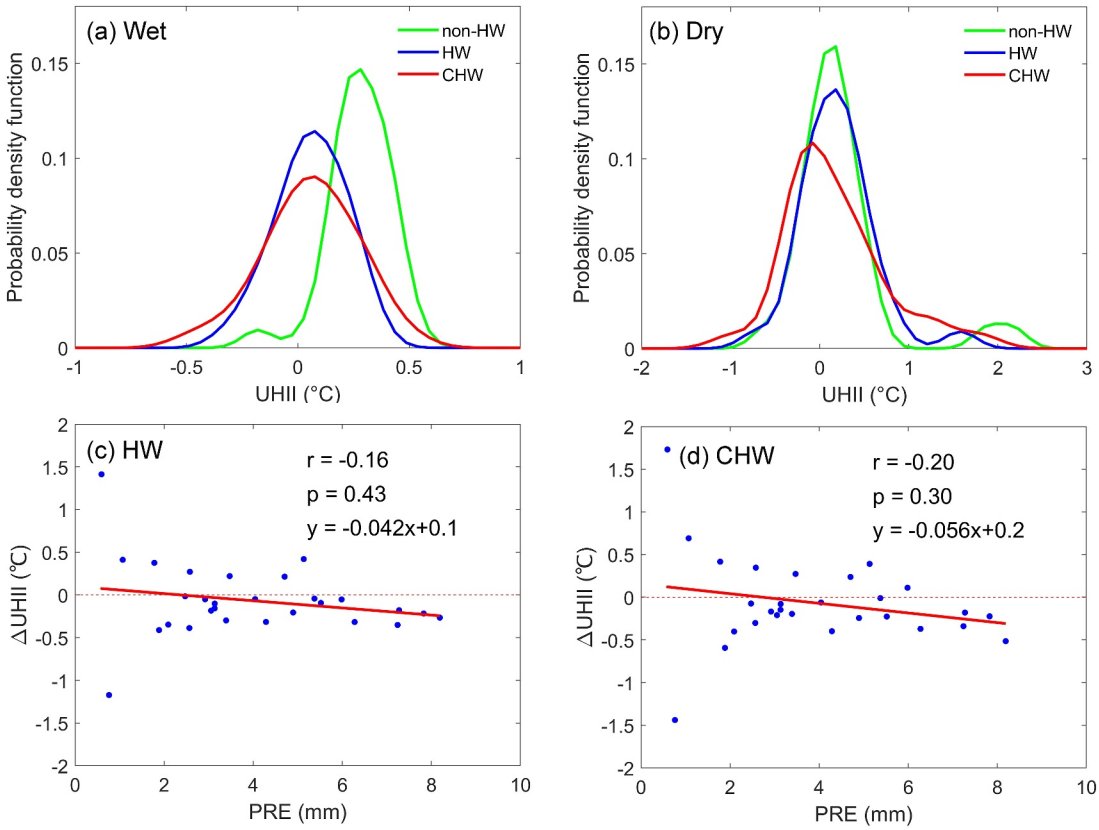

Figure 6. Probability distribution function of UHII during 1991–2021 in (a) a wet grid and (b) a dry grid. Correlation between mean ΔUHII and mean PRE during warm months under (c) HW conditions and (d) CHW conditions. Horizonal red dashed line represents the zero *x*-axis.

PRE exceeds 6 mm per day, negative ΔUHII values indicate a negative interaction between UHI and HW/CHW. Conversely, for most grids with PRE below 3 mm per day, ΔUHII is generally greater than or close to 0. The average ΔUHII is 0.01 and 0.02°C under HW/CHW conditions in dry grids, indicating a slightly positive interaction between UHI and HW/CHW. Additionally, in extremely dry areas (PRE <1 mm per day), the interaction between UHI and HW/CHW can vary significantly. For instance, UHII reduces by 1.17 and 1.44°C under HW/CHW conditions in the grid located at (80°–85°E, 40°–45°N), while UHII increases by 1.41 and 1.73°C under HW/CHW conditions in the grid at (85°–90°E, 40°–45°N). These discrepancies are partially attributed to the limited number of weather stations. Overall, these findings suggest an interaction between UHI and HW/CHW, with negative interactions in wet areas and positive interactions in dry regions.

4. Conclusions

In this study, we provide the first attempt to investigate the spatiotemporal characteristics of temporally compound HWs over mainland China with historical surface temperature data. Results reveal that CHWs constitute a larger portion of HW events during 1961–2021. The frequency and duration of CHWs increase much more significant in urban areas than in rural areas, especially in the southern parts of China. Compared with HWs, CHWs constitute more heat stress due to the prolonged extreme hot days. The increasing proportion of CHW days indicates that effective strategies are in urgent need to manage prolonged heat risks in cities. The finding is insensitive to the temperature threshold used to define hot days, but will change with the maximum, mean and minimum temperature. The largest percentage increase of CHW days from minimum temperatures indicates that heat stress is mostly intensified at night. UHIIs are found to be larger on non-HW days than under HW and CHW days over mainland China, though the effects of HW and CHW are different from region to region. Under HWs,

UHII will intensify in dry regions and weaken in wet regions. While CHW leads to a more dispersed distribution of UHII. During CHWs, UHIIs are the smallest during the cool break due to rainfall.

It needs to be noted that the present study has a few limitations. First, due to the lack of hourly data, only daily mean temperature data were used to investigate the interaction between UHI and CHWs. Jiang et al. (2019) found notable differences in the evolution of daytime UHI and nighttime UHI during HWs in Guangzhou, where UHII increases at night and decreases during the day. This indicates that the interaction between UHI and CHW could have large diurnal variations, which can not be reflected by the daily mean value in this study. Such variation could have adverse effects on nighttime urban environment because CHW may further intensify the large nighttime UHI and create extreme heat stress for outdoor citizens. Future studies shall be conducted to look into such diurnal variations with hourly data under different background climates. Second, various meteorological variables besides air temperature, such as humidity, wind speed and solar radiation, play important roles in influencing outdoor thermal stress. Compared to air temperature, heat indices that account for both air temperature and humidity suggest a larger thermal stress in most regions of China (P. Wang et al., 2021). It is therefore recommended to utilize various heat indices to advance the understanding of the impact of CHW on human health in the future. Third, given that CHW will become more frequent and last longer under future climates (Baldwin et al., 2019), analyzing future CHW hazards in urban regions under various emission scenarios will have large implications for sustainable development of cities. The Community Earth System Model (CESM) developed by the US National Center for Atmospheric Research is one of the few general circulation models that is capable of simulating near-surface urban air temperature. Running CESM simulation requires extensive computational resources beyond the scope of this study, but it is worth exploring in the future.

Conflict of Interest

The authors declare no conflicts of interest relevant to this study.

Data Availability Statement

Meteorological data that support the findings of this study are openly available at J. Yang (2025).

Acknowledgments
This work is supported by the National Natural Science Foundation of China for Excellent Young Scientists (42322903).

References

Anderson, G. B., & Bell, M. L. (2011). Heat waves in the United States: Mortality risk during heat waves and effect modification by heat wave characteristics in 43 U.S. communities. *Environmental Health Perspectives*, *119*(2), 210–218. https://doi.org/10.1289/ehp.1002313

Ao, X., Wang, L., Zhi, X., Gu, W., Yang, H., & Li, D. (2019). Observed synergies between urban heat islands and heat waves and their controlling factors in Shanghai, China. *Journal of Applied Meteorology and Climatology*, *58*(9), 1955–1972. https://doi.org/10.1175/JAMC-D-19-0073.1

Baldwin, J. W., Dessy, J. B., Vecchi, G. A., & Oppenheimer, M. (2019). Temporally compound heat wave events and global warming: An emerging hazard. *Earth's Future*, *7*(4), 411–427. https://doi.org/10.1029/2018EF000989

Ceccherini, G., Russo, S., Ameztoy, I., Marchese, A. F., & Carmona-Moreno, C. (2017). Heat waves in Africa 1981–2015, observations and reanalysis. *Natural Hazards and Earth System Sciences*, *17*(1), 115–125. https://doi.org/10.5194/nhess-17-115-2017

Chen, G., Chen, Y., He, H., Wang, J., Zhao, L., & Cai, Y. (2023). Assessing the synergies between heat waves and urban heat islands of different local climate zones in Guangzhou, China. *Building and Environment*, *240*, 110434. https://doi.org/10.1016/j.buildenv.2023.110434

Chen, M., Liu, W., & Tao, X. (2013). Evolution and assessment on China's urbanization 1960-2010: Under-urbanization or over-urbanization? *Habitat International*, *38*, 25–33. https://doi.org/10.1016/j.habitatint.2012.09.007

Chen, Y., & Zhai, P. (2017). Revisiting summertime hot extremes in China during 1961–2015: Overlooked compound extremes and significant changes. *Geophysical Research Letters*, *44*(10), 5096–5103. https://doi.org/10.1002/2016GL072281

Chew, L. W., Liu, X., Li, X.-X., & Norford, L. K. (2021). Interaction between heat wave and urban heat island: A case study in a tropical coastal city, Singapore. *Atmospheric Research*, *247*, 105134. https://doi.org/10.1016/j.atmosres.2020.105134

Deng, J. S., Wang, K., Hong, Y., & Qi, J. G. (2009). Spatio-temporal dynamics and evolution of land use change and landscape pattern in response to rapid urbanization. *Landscape and Urban Planning*, *92*(3–4), 187–198. https://doi.org/10.1016/j.landurbplan.2009.05.001

Ding, S., & Chen, A. (2024). Comprehensive assessment of daytime, nighttime and compound heatwave risk in east China. *Natural Hazards*, *120*(8), 7245–7263. https://doi.org/10.1007/s11069-024-06504-5

Jiang, S., Lee, X., Wang, J., & Wang, K. (2019). Amplified urban heat islands during heat wave periods. *Journal of Geophysical Research: Atmospheres*, *124*(14), 7797–7812. https://doi.org/10.1029/2018JD030230

Jyoteeshkumar Reddy, P., Perkins-Kirkpatrick, S. E., & Sharples, J. J. (2021). Intensifying Australian heatwave trends and their sensitivity to observational data. *Earth's Future*, *9*(4), e2020EF001924. https://doi.org/10.1029/2020EF001924

Kong, D., Gu, X., Li, J., Ren, G., & Liu, J. (2020). Contributions of global warming and urbanization to the intensification of human-perceived heatwaves over China. *Journal of Geophysical Research: Atmospheres*, *125*(18), e2019JD032175. https://doi.org/10.1029/2019JD032175

Li, D., & Bou-Zeid, E. (2013). Synergistic interactions between urban heat islands and heat waves: The impact in cities is larger than the sum of its parts. *Journal of Applied Meteorology and Climatology*, *52*(9), 2051–2064. https://doi.org/10.1175/JAMC-D-13-02.1

Li, D., Sun, T., Liu, M., Wang, L., & Gao, Z. (2016). Changes in wind speed under heat waves enhance urban heat islands in the Beijing metropolitan area. *Journal of Applied Meteorology and Climatology*, *55*(11), 2369–2375. https://doi.org/10.1175/JAMC-D-16-0102.1

Liao, W., Liu, X., Li, D., Luo, M., Wang, D., Wang, S., et al. (2018). Stronger contributions of urbanization to heat wave trends in wet climates. *Geophysical Research Letters*, *45*(20), 11310–11317. https://doi.org/10.1029/2018GL079679

Liu, F., Zhang, Z., Zhao, X., Liu, B., Wang, X., Yi, L., et al. (2021). Urban expansion of China from the 1970s to 2020 based on remote sensing technology. *Chinese Geographical Science*, *31*(5), 765–781. https://doi.org/10.1007/s11769-021-1225-5

Liu, J., Kuang, W., Zhang, Z., Xu, X., Qin, Y., Ning, J., et al. (2014). Spatiotemporal characteristics, patterns, and causes of land-use changes in China since the late 1980s. *Journal of Geographical Sciences*, *24*(2), 195–210. https://doi.org/10.1007/s11442-014-1082-6

Meque, A., Pinto, I., Maúre, G., & Beleza, A. (2022). Understanding the variability of heatwave characteristics in southern Africa. *Weather and Climate Extremes*, *38*, 100498. https://doi.org/10.1016/j.wace.2022.100498

Mitchell, D., Kornhuber, K., Huntingford, C., & Uhe, P. (2019). The day the 2003 European heatwave record was broken. *The Lancet Planetary Health*, *3*(7), e290–e292. https://doi.org/10.1016/S2542-5196(19)30106-8

Perkins-Kirkpatrick, S. E., & Lewis, S. C. (2020). Increasing trends in regional heatwaves. *Nature Communications*, *11*(1), 3357. https://doi.org/10.1038/s41467-020-16970-7

Perkins-Kirkpatrick, S. E., White, C. J., Alexander, L. V., Argüeso, D., Boschat, G., Cowan, T., et al. (2016). Natural hazards in Australia: Heatwaves. *Climatic Change*, *139*(1), 101–114. https://doi.org/10.1007/s10584-016-1650-0

Peterson, T. C., Heim, R. R., Hirsch, R., Kaiser, D. P., Brooks, H., Diffenbaugh, N. S., et al. (2013). Monitoring and understanding changes in heat waves, cold waves, floods, and droughts in the United States: State of knowledge. *Bulletin of the American Meteorological Society*, *94*(6), 821–834. https://doi.org/10.1175/BAMS-D-12-00066.1

Ramamurthy, P., & Bou-Zeid, E. (2017). Heatwaves and urban heat islands: A comparative analysis of multiple cities. *Journal of Geophysical Research: Atmospheres*, *122*(1), 168–178. https://doi.org/10.1002/2016JD025357

Ren, G., & Zhou, Y. (2014). Urbanization effect on trends of extreme temperature indices of national stations over mainland China, 1961–2008. *Journal of Climate*, *27*(6), 2340–2360. https://doi.org/10.1175/JCLI-D-13-00393.1

RESDC. (2024). Resources and environmental science data platform [Dataset]. *Data Center for Resources and Environmental Sciences, Chinese Academy of Sciences*. Retrieved from https://www.resdc.cn

Robine, J.-M., Cheung, S. L. K., Roy, S. L., Oyen, H. V., Griffiths, C., Michel, J.-P., & Herrmann, F. R. (2008). Death toll exceeded 70,000 in Europe during the summer of 2003. *Comptes Rendus Biologies*, *331*(2), 171–178. https://doi.org/10.1016/j.crvi.2007.12.001

Sarangi, C., Qian, Y., Li, J., Leung, L. R., Chakraborty, T. C., & Liu, Y. (2021). Urbanization amplifies nighttime heat stress on warmer days over the US. *Geophysical Research Letters*, *48*(24), e2021GL095678. https://doi.org/10.1029/2021GL095678

Sauter, C., Fowler, H. J., Westra, S., Ali, H., Peleg, N., & White, C. J. (2023). Compound extreme hourly rainfall preconditioned by heatwaves most likely in the mid-latitudes. *Weather and Climate Extremes*, *40*, 100563. https://doi.org/10.1016/j.wace.2023.100563

Stewart, I. D. (2011). A systematic review and scientific critique of methodology in modern urban heat island literature. *International Journal of Climatology*, *31*(2), 200–217. https://doi.org/10.1002/joc.2141

Thompson, V., Kennedy-Asser, A. T., Vosper, E., Lo, Y. T. E., Huntingford, C., Andrews, O., et al. (2022). The 2021 western North America heat wave among the most extreme events ever recorded globally. *Science Advances*, *8*(18), eabm6860. https://doi.org/10.1126/sciadv.abm6860

Tian, L., Lu, J., Li, Y., Bu, D., Liao, Y., & Wang, J. (2021). Temporal characteristics of urban heat island and its response to heat waves and energy consumption in the mountainous Chongqing, China. *Sustainable Cities and Society*, *75*, 103260. https://doi.org/10.1016/j.scs.2021.103260

Wang, J., Feng, J., Yan, Z., & Chen, Y. (2020). Future risks of unprecedented compound heat waves over three vast urban agglomerations in China. *Earth's Future*, *8*(12), e2020EF001716. https://doi.org/10.1029/2020EF001716

Wang, P., Luo, M., Liao, W., Xu, Y., Wu, S., Tong, X., et al. (2021). Urbanization contribution to human perceived temperature changes in major urban agglomerations of China. *Urban Climate*, *38*, 100910. https://doi.org/10.1016/j.uclim.2021.100910

Wang, P., Tang, J., Sun, X., Wang, S., Wu, J., Dong, X., & Fang, J. (2017). Heat waves in China: Definitions, leading patterns, and connections to large-scale atmospheric circulation and SSTs. *Journal of Geophysical Research: Atmospheres*, *122*(20), 10679–10699. https://doi.org/10.1002/2017JD027180

Wang, W., Zhou, W., Wang, X., Fong, S. K., & Leong, K. C. (2013). Summer high temperature extremes in southeast China associated with the East Asian jet stream and circumglobal teleconnection. *Journal of Geophysical Research: Atmospheres*, *118*(15), 8306–8319. https://doi.org/10.1002/jgrd.50633

White, R. H., Anderson, S., Booth, J. F., Braich, G., Draeger, C., Fei, C., et al. (2023). The unprecedented Pacific Northwest heatwave of June 2021. *Nature Communications*, *14*(1), 727. https://doi.org/10.1038/s41467-023-36289-3

Wu, S., Chan, T. O., Zhang, W., Ning, G., Wang, P., Tong, X., et al. (2021). Increasing compound heat and precipitation extremes elevated by urbanization in south China. *Frontiers in Earth Science*, *9*, 636777. https://doi.org/10.3389/feart.2021.636777

Wu, S., Luo, M., Zhao, R., Li, J., Sun, P., Liu, Z., et al. (2023). Local mechanisms for global daytime, nighttime, and compound heatwaves. *Npj Climate and Atmospheric Science*, *6*(1), 36. https://doi.org/10.1038/s41612-023-00365-8

Wu, X., Wang, L., Yao, R., Luo, M., Wang, S., & Wang, L. (2020). Quantitatively evaluating the effect of urbanization on heat waves in China. *Science of the Total Environment*, *731*, 138857. https://doi.org/10.1016/j.scitotenv.2020.138857

Xu, W., Li, Q., Wang, X. L., Yang, S., Cao, L., & Feng, Y. (2013). Homogenization of Chinese daily surface air temperatures and analysis of trends in the extreme temperature indices. *Journal of Geophysical Research: Atmospheres*, *118*(17), 9708–9720. https://doi.org/10.1002/jgrd.50791

Yan, M., Xie, Y., Zhu, H., Ban, J., Gong, J., & Li, T. (2022). The exceptional heatwaves of 2017 and all-cause mortality: An assessment of nationwide health and economic impacts in China. *Science of the Total Environment*, *812*, 152371. https://doi.org/10.1016/j.scitotenv.2021.152371

Yang, J. (2025). Temporally compound heatwave and its interaction with urban heat island over mainland China [Dataset]. *Zenodo*. https://doi.org/10.5281/zenodo.14994493

Yang, P., Ren, G., & Hou, W. (2019). Impact of daytime precipitation duration on urban heat island intensity over Beijing city. *Urban Climate*, *28*, 100463. https://doi.org/10.1016/j.uclim.2019.100463

Yao, R., Hu, Y., Sun, P., Bian, Y., Liu, R., & Zhang, S. (2022). Effects of urbanization on heat waves based on the wet-bulb temperature in the Yangtze River Delta urban agglomeration, China. *Urban Climate*, *41*, 101067. https://doi.org/10.1016/j.uclim.2021.101067

Ye, H., Huang, Z., Huang, L., Lin, L., & Luo, M. (2018). Effects of urbanization on increasing heat risks in south China. *International Journal of Climatology*, *38*(15), 5551–5562. https://doi.org/10.1002/joc.5747

You, Q., Jiang, Z., Kong, L., Wu, Z., Bao, Y., Kang, S., & Pepin, N. (2017). A comparison of heat wave climatologies and trends in China based on multiple definitions. *Climate Dynamics*, *48*(11), 3975–3989. https://doi.org/10.1007/s00382-016-3315-0

Zhao, L., Lee, X., Smith, R. B., & Oleson, K. (2014). Strong contributions of local background climate to urban heat islands. *Nature*, *511*(7508), 216–219. https://doi.org/10.1038/nature13462

Zhao, L., Oppenheimer, M., Zhu, Q., Baldwin, J. W., Ebi, K. L., Bou-Zeid, E., et al. (2018). Interactions between urban heat islands and heat waves. *Environmental Research Letters*, *13*(3), 034003. https://doi.org/10.1088/1748-9326/aa9f73

Zhou, W., Zhang, L., Zhang, Q., Li, Y., Wang, G., Tang, Z., et al. (2025). Decrease in urban-rural differences of nighttime humid heatwaves in the Yangtze River Delta, China. *Atmospheric Research*, *316*, 107956. https://doi.org/10.1016/j.atmosres.2025.107956